Parallel propagating modes and anomalous spatial damping in the ultra-relativistic electron plasma with arbitrary degeneracy

H Farooq[1], M Sarfraz[1], Z Iqbal[1], G Abbas[1,†], and H A Shah[2]

[1] *Department of Physics, Government College University, Lahore* 54000, *Pakistan*
[2] *Government College University, Lahore* 54000, *Pakistan*

(Received 12 May 2017; published online 30 September 2017)

The dispersion relations of parallel propagating modes (Langmuir mode, right and left handed circular polarized waves) in the weak magnetic field limit $|\omega - \boldsymbol{k}\cdot\boldsymbol{v}| \gg \Omega$ are considered for ultra-relativistic arbitrary degenerate electron plasma. The results are presented in terms of moments of Fermi–Dirac distribution. The increase in the electron equilibrium number density from negative large (weakly degenerate) to positive large (highly degenerate) values of μ/T_e is observed (where μ is the electron chemical potential and T_e is the electron thermal energy). As a result, shifting of the cutoff points in all the real dispersion branches towards the higher values and increasing in the band gap between unmagnetized longitudinal and transverse modes in k-space are examined. Also, the suppression of the weak magnetic field effects in weakly magnetized right handed and left handed circular polarized waves and a decrease in the longitudinal and transverse screening effects are observed in the graphical patterns due to an increase in the equilibrium number density.

Keywords: degenerate Fermi gases, relativistic plasmas, electromagnetic waves

PACS: 03.75.Ss, 52.27.Ny, 52.35.Hr **DOI:** 10.1088/1674-1056/26/11/110301

1. Introduction

Ultra-relativistic plasmas are formed either in the presence of strong electromagnetic fields or in extremely high temperatures. Such plasmas are believed to exist in the early universe or may be present in the neutron stars. Their signatures can also be found in a number of other environments, e.g., in a supernova explosion, in magnetars, in the accretion disks around black holes,[1,2] in high energy electron-radiation belts spiralling in Jupiter's magnetic field,[3] and in the orbital tracks of the Van Allen radiation belt around the earth.[4] Experimentally, they have also been detected in the vicinity of intense laser fields.[5]

The ultra-relativistic treatment of the non-degenerate or degenerate plasma waves can be found in the early literature. Silin[6] discussed the dispersion properties of electromagnetic waves for non-degenerate plasma, while Linhard[7] described them for fully degenerate plasma systems. The dynamics of highly relativistic non-degenerate plasma waves in pulsar atmospheres has been a topic of discussion in the recent literature.[8–10] In each case, the relativistic Maxwell–Boltzmann–Juttner distribution function[11] plays a key role in characterizing the behavior. On the other hand, Chandrasekhar[12] demonstrated the internal outward pressure (proportional to $n_e^{4/3}$) provided by the ultra-relativistic degenerate electron gas in white dwarf stars using the Fermi–Dirac equation of state. In recent years, many efforts have been made to understand the properties of linear and nonlinear waves in relativistic degenerate plasmas in the dense astrophysical objects.[13–15]

Plasma waves may also be discussed for the ideal electron gas at arbitrary degeneracy and relativity.[16] This occurs when the plasma particle temperature T approaches Fermi temperature T_F and the equilibrium distribution function changes from Maxwell–Boltzmann to the Fermi–Dirac distribution function. In this case, the choice of the parameter μ/T plays a crucial role, where μ is the chemical potential. The parameter is large and positive in the completely degenerate limit, and is large and negative in the non-degenerate limit. The literature on the arbitrary degenerate electron plasma waves is relatively sparse. Maafa[17] studied the ion acoustic and Langmuir waves with arbitrary degeneracy of electrons using the linearized classical kinetic theory. Eliasson and Shuklau[18] derived the nonlinear electron fluid equations for non-relativistic quantum plasmas including arbitrary electron degeneracy. Melrose and Mushtaq[19] calculated the longitudinal response function for arbitrary degenerate thermal electron gas. Such arbitrary degeneracy may also be important in the extreme relativistic case, e.g., in the earlier work on relativistic degenerate plasma waves, Melrose and Hayes[20] extended Jancovici's results[21] to the nearly degenerate limit and Tsytovich's results[22] to a mildly degenerate plasma.

In our earlier calculations, the dispersion properties of high frequency relativistic parallel and perpendicular propagating non-degenerate[23,24] and degenerate[25,26] electron plasma waves have been derived and discussed under a weak magnetic field condition $|\omega - \boldsymbol{k}\cdot\boldsymbol{v}| \gg \Omega$. In the present case, we aim to investigate the dispersion properties of parallel propagating plasma waves by considering the following as-

†Corresponding author. E-mail: gohar.abbas@gcu.edu.pk

sumptions: (i) ultra-relativistic ideal electron gas in which the rest mass energy is much smaller than the thermal energy, (ii) arbitrary electron degeneracy, and (iii) isotropic distribution. We also discuss our results in the two limiting cases: (i) the superluminal limit $\omega > ck$ that corresponds to the results near plasma oscillations and (ii) the subluminal limit $\omega < ck$ where the longitudinal fields are screened out and the transverse fields penetrate into the medium. In this paper, we restrict ourselves to conditions where the ions behave classically, which is the case in most astrophysical situations.

The paper is arranged as follows. Section 2 describes the mathematical derivation and analytical discussion of graphical results of unmagnetized longitudinal and transverse modes and weakly magnetized circularly polarized waves using a generalized ultra-relativistic Fermi–Dirac distribution function. Section 3 summaries the results and discussion.

2. Dispersion relations of parallel propagating waves in a weak magnetic field limit

In this section, we present the dispersion properties of parallel propagating modes (Langmuir mode and right and left handed circular polarized waves) for ultra-relativistic electron plasma. Ions are considered as fixed and forming the neutralizing background. Knowing the system of kinetic equations along with Maxwell's equations, the dispersion relations of electromagnetic right and left handed circular polarized (R- & L-) waves and electrostatic (Langmuir) waves are respectively given by

$$\omega^2 - c^2k_\parallel^2 + \Pi_{xx} \pm \mathrm{i}\Pi_{xy} = 0, \tag{1}$$

$$\omega^2 + \Pi_{zz} = 0. \tag{2}$$

The components Π_{xx}, Π_{yy}, Π_{xy}, and Π_{zz} have been calculated previously[24,27] assuming an isotropic particle distribution in a weak magnetic field limit $|\omega - \boldsymbol{k}\cdot\boldsymbol{v}| \gg \Omega$:

$$\begin{aligned}\Pi_{xx} &= \Pi_{yy} = \frac{8\pi^2e^2\omega^2}{k_\parallel^2}\int_0^\infty \frac{p^2}{v}\frac{\partial f_0}{\partial p}\mathrm{d}p \\ &\times\left[1 - \frac{\omega^2 - k_\parallel^2v^2}{2\omega k_\parallel v}\log\left|\frac{\omega + k_\parallel v}{\omega - k_\parallel v}\right| \right. \\ &\left. - \frac{\mathrm{i}\pi k_\parallel v}{2\omega}\left(1 - \frac{\omega^2}{k_\parallel^2v^2}\right)H\left(1 - \frac{\omega}{k_\parallel v}\right)\right],\end{aligned} \tag{3}$$

$$\begin{aligned}\Pi_{xy} &= -\frac{16\pi^2\mathrm{i}e^2\omega}{k_\parallel^2}\int_0^\infty \frac{p^2}{v}\Omega\frac{\partial f_0}{\partial p}\mathrm{d}p \\ &\times\left[1 - \frac{\omega}{2k_\parallel v}\log\left|\frac{\omega + k_\parallel v}{\omega - k_\parallel v}\right| \right. \\ &\left. - \frac{\mathrm{i}\pi k_\parallel v}{4}\frac{\partial}{\partial\omega}\left(1 - \frac{\omega^2}{k_\parallel^2v^2}\right)H\left(1 - \frac{\omega}{k_\parallel v}\right)\right],\end{aligned} \tag{4}$$

$$\begin{aligned}\Pi_{zz} &= -\frac{16\pi^2e^2\omega^2}{k_\parallel^2}\int_0^\infty \frac{p^2}{v}\frac{\partial f_0}{\partial p}\mathrm{d}p \\ &\times\left[1 - \frac{\omega}{2k_\parallel v}\log\left|\frac{\omega + k_\parallel v}{\omega - k_\parallel v}\right| + \frac{\mathrm{i}\pi\omega}{2k_\parallel v}H\left(1 - \frac{\omega}{k_\parallel v}\right)\right],\end{aligned} \tag{5}$$

where $k_\parallel$ is the propagation parallel to the ambient magnetic field $\boldsymbol{B}_0 = \left(0, 0, B_{0z}\right)$, and Ω is the non-relativistic cyclotron frequency. The unit step function $H\left(1 - \frac{\omega}{k_\parallel v}\right) = 0$ for $\frac{\omega}{k_\parallel v} > 1$ and $H\left(1 - \frac{\omega}{k_\parallel v}\right) = 1$ in the limit $\frac{\omega}{k_\parallel v} \leqslant 1$. In Eqs. (3)–(5), the pole contributions are explicitly presented in order to get spatial (or temporal) damping (or growth). The components have been used in calculating the dispersion relations of fully relativistic high frequency non-degenerate[24] and degenerate[25] electron plasma waves and the anomalous spatial damping in the limit $\frac{\omega}{k_\parallel v} < 1$.[27,28] We now proceed to derive the dispersion relations of parallel propagating waves in ultra-relativistic electron plasma for arbitrary degeneracy. In this case, the relativistic factor $\gamma = \sqrt{1 + p^2/m_0^2c^2}$ is approximated to $\gamma \simeq p/m_0c$. As a result, the plasma frequency and the cyclotron frequency become $\omega_\mathrm{p} = \sqrt{\frac{4\pi n_0e^2c}{|p|}}$ and $\Omega = \frac{eB_0}{|p|}$. Also the polarization tensor components equations (3)–(5) become

$$\begin{aligned}\Pi_{xx} &= \Pi_{yy} = \frac{8\pi^2e^2\omega^2}{k_\parallel^2}\int_0^\infty \frac{p^2}{c}\frac{\partial f_0}{\partial p}\mathrm{d}p \\ &\times\left[1 - \frac{\omega^2 - k_\parallel^2c^2}{2\omega k_\parallel c}\log\left|\frac{\omega + k_\parallel c}{\omega - k_\parallel c}\right| \right. \\ &\left. - \frac{\mathrm{i}\pi k_\parallel c}{2\omega}\left(1 - \frac{\omega^2}{k_\parallel^2c^2}\right)H\left(1 - \frac{\omega}{k_\parallel c}\right)\right],\end{aligned} \tag{6}$$

$$\begin{aligned}\Pi_{xy} &= -\frac{16\pi^2\mathrm{i}e^2\omega}{k_\parallel^2}\int_0^\infty \frac{p^2}{c}\frac{eB_0}{p}\frac{\partial f_0}{\partial p}\mathrm{d}p \\ &\times\left[1 - \frac{\omega}{2k_\parallel c}\log\left|\frac{\omega + k_\parallel c}{\omega - k_\parallel c}\right| \right. \\ &\left. - \frac{\mathrm{i}\pi k_\parallel c}{4}\frac{\partial}{\partial\omega}\left(1 - \frac{\omega^2}{k_\parallel^2c^2}\right)H\left(1 - \frac{\omega}{k_\parallel c}\right)\right],\end{aligned} \tag{7}$$

$$\begin{aligned}\Pi_{zz} &= -\frac{16\pi^2e^2\omega^2}{k_\parallel^2}\int_0^\infty \frac{p^2}{c}\frac{\partial f_0}{\partial p}\mathrm{d}p \\ &\times\left[1 - \frac{\omega}{2k_\parallel c}\log\left|\frac{\omega + k_\parallel c}{\omega - k_\parallel c}\right| + \frac{\mathrm{i}\pi\omega}{2k_\parallel c}H\left(1 - \frac{\omega}{k_\parallel c}\right)\right].\end{aligned} \tag{8}$$

We now choose the Fermi–Dirac distribution function for the particles having ultra-relativistic energy $E = cp$

$$f_0^\mathrm{e} = \frac{2}{(2\pi)^3}\frac{1}{z^{-1}\,\mathrm{e}^{cp/T_\mathrm{e}} + 1}, \tag{9}$$

where $z^{-1} = \exp[-\mu/T_\mathrm{e}]$ is the fugacity of the electron; μ is the chemical potential, c is the velocity of light in a vacuum, and $T_\mathrm{e} = k_\mathrm{B}T$ is the electron thermal energy. Here the customary Boltzmann constant k_B is omitted as we are working in cgs units. The equilibrium number density associated with the Fermi–Dirac distribution function is

$$n_{0\mathrm{e}(\mu/T_\mathrm{e})} = \frac{8\pi}{(2\pi)^3}\int_0^\infty \frac{p^2\mathrm{d}p}{\mathrm{e}^{cp/T_\mathrm{e} - \mu/T_\mathrm{e}} + 1}$$

$$= -\frac{2}{\pi^2}\frac{T_e^3}{c^3} Li_{3(\mu/T_e)}, \tag{10}$$

where we have used

$$\int_0^\infty \frac{dx x^n}{z^{-1}e^x+1} = -\Gamma(n+1)\, Li_n(-z). \tag{11}$$

Here, μ/T_e, represented in the subscript of the electron number density in Eq. (10), is for the arbitrary degeneracy dependence and $Li_{3(\mu/T_e)}$ $(= Li_3(-e^{\mu/T_e}))$ is the Polylog function of order 3. The Polylog function has the power series expansion in the non degenerate limit $z = e^{\mu/T_e} \ll 1$

$$Li_n(z) = \sum_{s=1}^{\infty} \frac{z^s}{s^n}, \tag{12}$$

and the asymptotic expansion in the completely degenerate limit $z = e^{\mu/T_e} \gg 1$

$$-\lim_{z->\infty} \Gamma(n+1) Li_n(-z) = (\ln z)^n. \tag{13}$$

The expansions (Eqs. (12) and (13) may be regarded as alternative definitions of $Li_n(-z)$, and have been used by a number of authors (see e.g., Refs. [18] and [19]) to obtain the approximate results of the waves with arbitrary degeneracy. Under this scenario, different environments for ultra-relativistic electron plasma gas ranging from under dense to ultra-dense regimes can be approximated. The chemical potential μ can be obtained numerically from Eq. (10). To compute the integral numerically over the Polylog function, we use Mathematica (V.9), which is capable of calculating generalized Polylog functions. The approximated values of the ratios μ/E_F, T/T_F, μ/T_e, and z are tabulated below:

$$\begin{bmatrix} \frac{\mu}{E_F} & 1.0 & 0.64 & 0.5 & 0 & -0.78 & -1.83 & -2.12 \\ \frac{T}{T_F} & 0 & 0.32 & 0.39 & 0.56 & 0.78 & 1 & 1.06 \\ \mu/T_e & \infty & 2.0 & 1.28 & 0 & -1 & -1.83 & -2.0 \\ z = e^{\mu/T_e} & \infty & 7.38 & 3.59 & 1 & 0.36 & 0.16 & 0.13 \end{bmatrix}. \tag{14}$$

We have also plotted the normalized equilibrium number density $n_{0(\mu/T_e)}/n_{0(0)}$ in Fig. 1 for different μ/T_e, which shows a decreasing trend for $\mu/T_e < 0$ and vise versa for $\mu/T_e > 0$. We now apply the Fermi–Dirac distribution function (Eq. (9)) in the above set of equations (Eqs. (6)–(8)) and obtain the following integral results:

$$\begin{aligned} \int_0^\infty p^2 \frac{\partial f_0}{\partial p} dp &= \frac{4}{(2\pi)^3}\frac{T_e^2}{c^2} Li_{2(\mu/T_e)}, \\ \int_0^\infty p \frac{\partial f_0}{\partial p} dp &= \frac{2}{(2\pi)^3}\frac{T_e}{c} Li_{1(\mu/T_e)}, \\ \int_0^\infty \frac{\partial f_0}{\partial p} dp &= \frac{2}{(2\pi)^3} Li_{0(\mu/T_e)}, \end{aligned} \tag{15}$$

where we have used the following expression:

$$\int_0^\infty dp\, p^n \frac{\partial f_0^e}{\partial p} = \frac{2}{(2\pi)^3}\left(\frac{T_e}{c}\right)^n \Gamma(n+1)\, Li_n(-e^{\mu/T_e}). \tag{16}$$

The equilibrium number density Eq. (10) over the volume element can also be obtained from Eq. (16). Plugging Eqs. (15) and (10) back into Eqs. (6)–(8), we obtain

$$\begin{aligned} \Pi_{xx} = \Pi_{yy} &= -\frac{3}{2}\frac{\omega^2}{c^2 k_\parallel^2}\omega_{pe}^2 \frac{Li_{2(\mu/T_e)}}{Li_{3(0)}} \\ &\times \left[1 - \frac{\omega^2 - k_\parallel^2 c^2}{2\omega k_\parallel c}\log\left|\frac{\omega + k_\parallel c}{\omega - k_\parallel c}\right| \right. \\ &\left. - \frac{i\pi k_\parallel c}{2\omega}\left(1 - \frac{\omega^2}{k_\parallel^2 c^2}\right) H\left(1 - \frac{\omega}{k_\parallel c}\right)\right], \end{aligned} \tag{17}$$

$$\begin{aligned} \Pi_{xy} &= 3\frac{i\omega}{c^2 k_\parallel^2}\omega_{pe}^2 \omega_{ce} \frac{Li_{1(\mu/T_e)}}{Li_{3(0)}} \\ &\times \left[1 - \frac{\omega}{2k_\parallel c}\log\left|\frac{\omega + k_\parallel c}{\omega - k_\parallel c}\right| \right. \\ &\left. - \frac{i\pi k_\parallel c}{4}\frac{\partial}{\partial\omega}\left(1 - \frac{\omega^2}{k_\parallel^2 c^2}\right) H\left(1 - \frac{\omega}{k_\parallel c}\right)\right], \end{aligned} \tag{18}$$

$$\begin{aligned} \Pi_{zz} &= 3\frac{\omega^2}{c^2 k_\parallel^2}\omega_{pe}^2 \frac{Li_{2(\mu/T_e)}}{Li_{3(0)}}\left[1 - \frac{\omega}{2k_\parallel c}\log\left|\frac{\omega + k_\parallel c}{\omega - k_\parallel c}\right| \right. \\ &\left. + \frac{i\pi\omega}{2k_\parallel c} H\left(1 - \frac{\omega}{k_\parallel c}\right)\right], \end{aligned} \tag{19}$$

where $\omega_{pe} = \sqrt{\frac{4\pi n_{0e} c^2 e^2}{3T_e}}$ and $\omega_{ce} = \frac{eB_0 c}{T_e}$. Here we have fixed the electron density n_{0e} given in the definition of electron plasma frequency for $\mu/T_e = 0$. The Polylog functions written in the above components (Eqs. (17)–(19)) can be read as $\frac{Li_{2(\mu/T_e)}}{Li_{3(0)}} = \frac{Li_2(-e^{\mu/T_e})}{Li_3(-1)}$ and $\frac{Li_{1(\mu/T_e)}}{Li_{3(0)}} = \frac{Li_1(-e^{\mu/T_e})}{Li_3(-1)}$. The graphical representation of the factors $\frac{Li_{2(\mu/T_e)}}{Li_{3(0)}}$ (associated with unmagnetized Π_{zz} and Π_{xx} components) and $\frac{Li_{1(\mu/T_e)}}{Li_{3(0)}}$ (with the weakly magnetized Π_{xy} component) is given in Fig. 2 for different μ/T_e. Observe that, for the large negative values of μ/T_e (i.e., $\mu/T_e < -1$), the curves of $\frac{Li_{2(\mu/T_e)}}{Li_{3(0)}}$ (red) and $\frac{Li_{1(\mu/T_e)}}{Li_{3(0)}}$ (blue) merge together and lead to the dispersion relations of non-degenerate (Boltzmann) plasma gas. Merging of the curves means $\frac{Li_{2(\mu/T_e)}}{Li_{3(0)}} \simeq \frac{Li_{1(\mu/T_e)}}{Li_{3(0)}}$. Another cross check can be done by fixing the plasma frequency for $\mu/T_e = -15$ (for example). In this case, the ratios $\frac{Li_{2(-15)}}{Li_{3(-15)}}$ and $\frac{Li_{1(-15)}}{Li_{3(-15)}}$ approach unity. The prominent difference between the curves starts

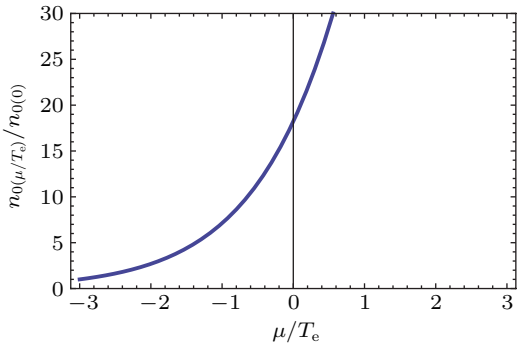

Fig. 1. (color online) Normalized electron equilibrium number density $\frac{n_{0(\mu/T_e)}}{n_{0(0)}}$ as a function of $\frac{\mu}{T_e}$ (where $n_{0(0)}$ corresponds to $\frac{\mu}{T_e} = 0$).

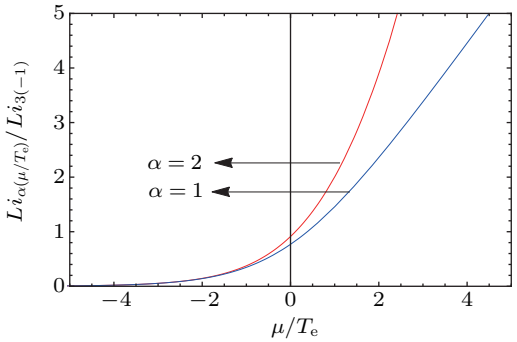

Fig. 2. (color online) $\frac{Li_{\alpha(\mu/T_e)}}{Li_{3(0)}}$ vs. μ/T_e, showing the graphical trend of the Polylog functions $\frac{Li_{2(\mu/T_e)}}{Li_{3(0)}}$ (red) and $\frac{Li_{1(\mu/T_e)}}{Li_{3(0)}}$ (blue) associated with unmagnetized and weakly magnetized tensor components with $\frac{\mu}{T_e}$. At negative and large value of $\frac{\mu}{T_e}$, the curves merge and $\frac{Li_{2(\mu/T_e)}}{Li_{3(0)}} \simeq \frac{Li_{1(\mu/T_e)}}{Li_{3(0)}}$.

from the values $\mu/T_e \geqslant -1$ where the numerical strength of the factor $\frac{Li_{2(\mu/T_e)}}{Li_{3(0)}}$ becomes larger as compared to $\frac{Li_{1(\mu/T_e)}}{Li_{3(0)}}$. We now proceed to derive the dispersion relations of unmagnetized and weakly magnetized parallel propagating arbitrary degenerate electron plasma waves.

2.1. Dispersion relations of ultra-relativistic unmagetized electron plasma waves with arbitrary degeneracy

First, we present the dispersion relations of ultra-relativistic unmagnetized electron plasma waves. We ignore the contribution of Π_{xy} associated with an ambient magnetic field. Using Eq. (16) in Eq. (1) and Eq. (19) in Eq. (2), we respectively obtain unmagnetized longitudinal and transverse modes

$$\omega^2 + 3\omega_{pe}^2 \frac{\omega^2}{c^2k_\parallel^2}\frac{Li_{2(\mu/T_e)}}{Li_{3(0)}}\left[1 - \frac{\omega}{2k_\parallel c}\log\left|\frac{\omega + k_\parallel c}{\omega - k_\parallel c}\right| + \frac{i\pi\omega}{2k_\parallel c}H\left(1 - \frac{\omega}{k_\parallel c}\right)\right] = 0, \tag{20}$$

$$\omega^2 - c^2k_\parallel^2 - \frac{3}{2}\frac{\omega^2}{c^2k_\parallel^2}\omega_{pe}^2\frac{Li_{2(\mu/T_e)}}{Li_{3(0)}} \times \left[1 - \frac{\omega^2 - k_\parallel^2c^2}{2\omega k_\parallel c}\log\left|\frac{\omega + k_\parallel c}{\omega - k_\parallel c}\right| - \frac{i\pi k_\parallel c}{2\omega}\left(1 - \frac{\omega^2}{k_\parallel^2c^2}\right)H\left(1 - \frac{\omega}{k_\parallel c}\right)\right] = 0. \tag{21}$$

Figure 3 shows the graphical representation of the principal part of Eqs. (20) and (21) for $\mu/T_e = -2$ (red), 0 (green), 2 (black). In all three cases, the upper curves are for transverse waves while the lower ones are for longitudinal waves. By increasing μ/T_e, the following three changes in the behavior of longitudinal (lower curve) and transverse (upper curve) waves occur. (i) The cutoff frequencies shift upward, (ii) the band width between longitudinal and transverse modes in k-space increases, and (iii) the wave propagation becomes weaker for larger values of μ/T_e. In case of highly degenerate plasma ($\mu/T_e \gg 0$), this occurs due to the higher electron density. In the following, we present the above equations in two limiting cases.

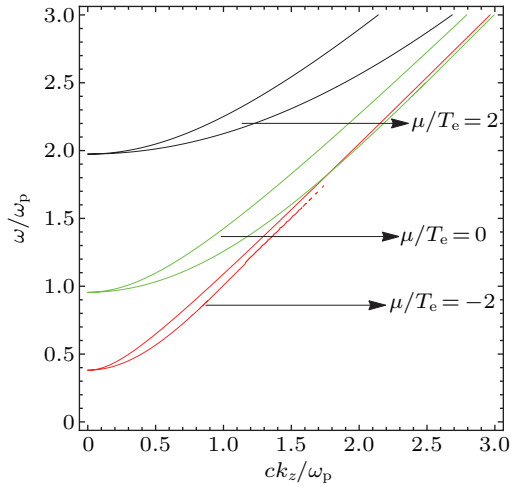

Fig. 3. (color online) Longitudinal (lower curves) and transverse (upper curves) modes for $\frac{\mu}{T_e} = -2$ (red), 0 (green), and 2 (black).

2.1.1. Superluminal $\omega/k_\parallel \gg c$ and subluminal $\omega/k_\parallel \ll c$ limiting cases

It follows immediately that the imaginary parts of Eqs. (21) and (22) vanish for $\omega/k_\parallel \gg c$ and absorption of wave is impossible in this case. In this limit, the frequency spectra can be approximated to give the dispersion relations near plasma oscillations

$$\omega^2 = \omega_p^2\frac{Li_{2(\mu/T_e)}}{Li_{3(0)}} + \frac{3}{5}c^2k_\parallel^2, \tag{22}$$

$$\omega^2 = \omega_p^2\frac{Li_{2(\mu/T_e)}}{Li_{3(0)}} + \frac{6}{5}c^2k_\parallel^2, \tag{23}$$

where we have expanded the logarithmic terms up to the second order in $ck_\parallel/\omega$. On the other hand, in the range of small phase velocities (i.e., in the limit $\omega/k_\parallel \ll c$), the waves are either strongly screened or absorbed. Under this condition, equation (20) reduces to

$$1 + 3\frac{\omega_p^2}{c^2k_\parallel^2}\frac{Li_{2(\mu/T_e)}}{Li_{3(0)}}\left[1 + \frac{i\pi\omega}{2k_\parallel c}\right] = 0. \tag{24}$$

Neglecting the imaginary term under the limit, $\omega < k_\parallel c$, we obtain the following expression of the Debye screening length:

$$\left(\lambda_D\right)_{\frac{\mu}{T_e}} = \left(\frac{c^2}{3\omega_p^2}\frac{Li_{3(0)}}{Li_{2(\mu/T_e)}}\right)^{1/2}. \tag{25}$$

In the case of non-relativistic electron–ion plasma, the screening length depends on the particle mass and thermal temperature. In the ultra-relativistic range, it depends on the thermal energies which are much larger than the rest mass energy. In the earlier calculation,[27] it was observed that the screening length increases with the increase of relativistic effects. In the present case of ultra-relativistic arbitrary degeneracy, the variation of screening length $(\lambda_D)_{\frac{\mu}{T_e}}$ in Eq. (25) with respect to

μ/T_e is shown in Fig. 4. This can also be considered as the inverse graph (red curve) of $\frac{Li_{2(\mu/T_e)}}{Li_{3(0)}}$ plotted in Fig. 2. The physical picture is clear from the figure that shows the larger screening length in weakly-degenerate environments as compared to the other ones.

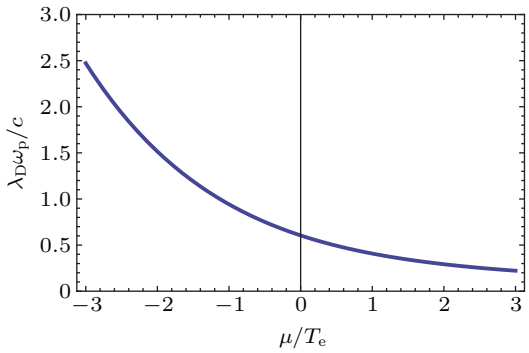

Fig. 4. (color online) Normalized Debye screening length $\frac{\lambda_D\omega_p}{c}$ as a function of $\frac{\mu}{T_e}$.

Anomalous skin effects In a collisionless plasma having a high frequency in range $\omega_p \gg \omega \gg \nu$ (collision frequency), the constant local collisionless skin depth is determined by electron inertia $\delta_l = c/\omega_{pe}$. When the wave phase speed becomes smaller than the particle thermal speed, then the conductivity becomes a function of ω throughout the entire skin layer and is known as anomalous. The relativistic treatment of anomalous penetration depth has been studied for non-degenerate[27] and fully degenerate plasmas.[28] To describe its behavior for arbitrary degeneracy, we neglect the principal logarithmic part given in Eq. (21) under the approximation $c^2k_\parallel^2 \gg \omega^2, \omega_p^2$, and obtain

$$\frac{c^2k_\parallel^2}{\omega^2} \simeq 3\frac{\omega_p^2}{c^2k_\parallel^2}\frac{Li_{2(\mu/T_e)}}{Li_{3(0)}}\left(\frac{i\pi k_\parallel c}{2\omega}\right), \tag{26}$$

or

$$k_\parallel^3 = i\pi\frac{3}{4}\frac{\omega}{c^3}\omega_p^2\left(\frac{Li_{2(\mu/T_e)}}{Li_{3(0)}}\right). \tag{27}$$

Equation (27) is cubic in $k_\parallel$ and has three roots, two of them are complex conjugate having the form $(\pm a + ib)$ and one is purely imaginary. The space scale of damping $(\lambda_{sk})_{\frac{\mu}{T_e}}$ of electromagnetic waves obtained from the imaginary part of the two complex roots in $k_\parallel$ is given by

$$(\lambda_{sk})_{\frac{\mu}{T_e}} = \frac{1}{\mathrm{Im}\,k_\parallel} = 2\left(\frac{4}{3\pi}\frac{c^3}{\omega\omega_p^2}\frac{Li_{3(0)}}{Li_{2(\mu/T_e)}}\right)^{1/3}. \tag{28}$$

Graphical analysis of Eq. (28) is given in Fig. 5, which shows the larger penetration depth of the electromagnetic waves in weakly-degenerate ($\mu/T_e < 0$) plasma regimes as compared to partially or fully degenerate ones. The graphical results also confirm the pattern observed in our previous study (Fig. 1 in Ref. [28]). In the following subsection, we proceed to analyze the parallel propagating electromagnetic waves in a weakly magnetized plasma.

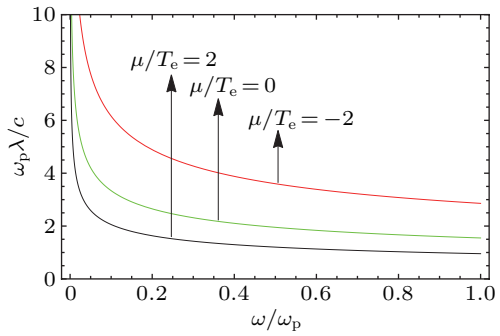

Fig. 5. (color online) Unmagnetized normalized skin depth $\frac{\lambda_{sk}\omega_p}{c}$ vs. deriving frequency $\frac{\omega}{\omega_p}$ for $\frac{\mu}{T_e} = -2$ (red), 0 (green), and 2 (black).

2.2. Ultra-relativistic weakly magnetized circular polarized waves with arbitrary degeneracy

Using Eqs. (17) and (18) in Eq. (2), we obtain the dispersion relations of R- & L-waves for a degenerate ultra-relativistic electron plasma

$$\begin{aligned}
&\omega^2 - c^2k_\parallel^2 - \frac{3}{2}\frac{\omega^2}{c^2k_\parallel^2}\omega_p^2\left(\frac{Li_{2(\mu/T_e)}}{Li_{3(0)}}\right)\\
&\times\left[1 - \frac{\omega^2 - k_\parallel^2c^2}{2\omega k_\parallel c}\log\left|\frac{\omega + k_\parallel c}{\omega - k_\parallel c}\right|\right.\\
&\left.- \frac{i\pi k_\parallel c}{2\omega}\left(1 - \frac{\omega^2}{k_\parallel^2c^2}\right)H\left(1 - \frac{\omega}{k_\parallel c}\right)\right]\\
&\mp 3\frac{\omega}{c^2k_\parallel^2}\frac{Li_{1(\mu/T_e)}}{Li_{3(0)}}\omega_p^2\omega_c\left[1 - \frac{\omega}{2k_\parallel c}\log\left|\frac{\omega + k_\parallel c}{\omega - k_\parallel c}\right|\right.\\
&\left.- \frac{i\pi k_\parallel c}{4}\frac{\partial}{\partial\omega}\left(1 - \frac{\omega^2}{k_\parallel^2c^2}\right)H\left(1 - \frac{\omega}{k_\parallel c}\right)\right] = 0,
\end{aligned} \tag{29}$$

where the $\mp$ signs are for the R- & L-waves, respectively. In our earlier calculations,[24,25] the suppression of the weak ambient magnetic field was observed with the addition of relativistic effects. In the present case, we observe how the constant ambient field strength is affected by the variation of the parameter μ/T_e. In Fig. 6, the upper/lower parts of red, green, and black curves show the corresponding representation of R/L-waves for $\mu/T_e = -2, 0, 2$. The difference of the left (lower) and right (upper) cut-off points (red curves for $\mu/T_e = -2$) (though quantitatively small in ultra-relativistic regimes) is larger in case of weakly degenerate environments as compared to other (partially (green) or strongly (black)) degenerate ones. This indicates that, the strength of the ambient magnetic field becomes weaker, as we move from weakly to strongly degenerate ultra-relativistic electron plasma regions.

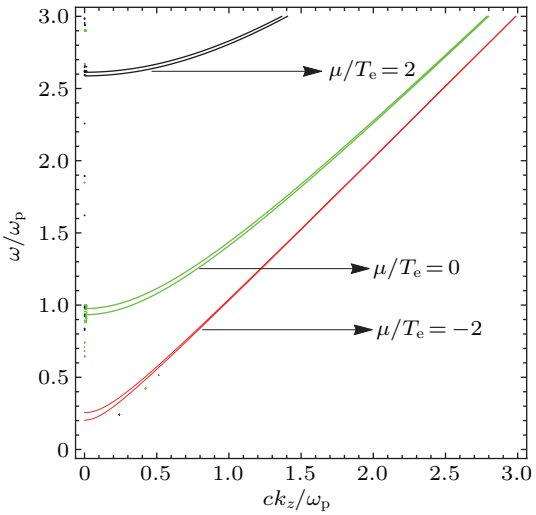

Fig. 6. (color online) $\frac{\omega}{\omega_p}$ vs. $\frac{ck_z}{\omega_p}$, showing the behavior of R-wave (upper curves) and L-wave (lower curves) for $\frac{\mu}{T_e} = -2$ (red), 0 (green), and 2 (black) at $\frac{\omega_c}{\omega_p} = 0.05$.

In the frequency range near the plasma oscillations, i.e., $\omega^2 \gg c^2k_\parallel^2$ and $\omega^2 \approx \omega_p^2 \frac{Li_{2(\mu/T_e)}}{Li_{3(0)}}$, the frequency spectra of the circular polarized waves in a weak magnetic field limit take the form

$$\omega^2 = \omega_p^2 \frac{Li_{2(\mu/T_e)}}{Li_{3(0)}} + \frac{6}{5}c^2k_\parallel^2 \pm \frac{1}{2}\frac{\omega_c}{\omega}\omega_p^2 \frac{Li_{1(\mu/T_e)}}{Li_{3(0)}}. \quad (30)$$

Ignoring the propagation, the above two equations (Eq. (30)) become cubic in ω and have two physical roots given by

$$\omega, \omega' = \sqrt{\omega_p^2\left(\frac{Li_{2(\mu/T_e)}}{Li_{3(0)}}\right)} \pm \frac{1}{2}\omega_c\left(\frac{Li_{1(\mu/T_e)}}{Li_{2(\mu/T_e)}}\right), \quad (31)$$

where ω and ω' are the oscillations represented as a function of the parameter μ/T_e. The graphical trend of the normalized right handed ω/ω_p (solid lines) and left handed ω'/ω_p (dashed lines) oscillations is shown in Fig. 7 for $\omega_c/\omega_p = 0.1$ (red), 0.05 (green), and 0.01 (black). Observe that the separation of the right-handed (solid) and left-handed (dotted) frequency curves due to the variation in the parameter ω_c/ω_p being more prominent in the weakly degenerate range (i.e., $\mu/T_e < 0$) and goes on decreasing for $\mu/T_e \geqslant 0$.

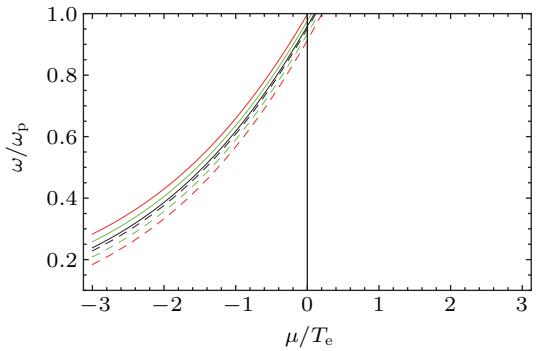

Fig. 7. (color online) Normalized $\frac{\omega}{\omega_p}, \frac{\omega'}{\omega_p}$ (right-hand (solid), left-hand (dashed)) oscillations as a function $\frac{\mu}{T_e}$ for $\frac{\omega_c}{\omega_p} = 0.01$ (red), 0.05 (green), and 0.1 (black).

Transverse penetration in a weakly magnetized electron plasma In the following, we examine the behavior of electromagnetic waves in a weakly magnetized ultra-relativistic plasma in the range of small phase velocities for arbitrary degeneracy. As done in the previous subsection, we apply approximation $c^2k_\parallel^2 \gg \omega^2, \omega_p^2$ in Eq. (29), neglect the principal part, and obtain the following equation quintic in $k_\parallel$:

$$k_\parallel^5 = \frac{3i\pi}{4}\left[k_\parallel^2\frac{\omega\omega_p^2}{c^3}\left(\frac{Li_{2(\mu/T_e)}}{Li_{3(0)}}\right) \pm \frac{\omega_p^2}{c^5}\omega_c\omega^2\left(\frac{Li_{1(\mu/T_e)}}{Li_{3(0)}}\right)\right]. \quad (32)$$

Previously, the field penetration of the parallel propagating waves in a relativistic plasma has been discussed using Jutner distribution function[27] and a comparison has been made with the results obtained in a relativistic degenerate plasma.[28] Solving Eq. (32) numerically, we obtain five roots, one pure imaginary and four complex having the form $-ie, (\pm a' + ib'), (\pm c - id)$. Like the unmagnetized case (Eq. (28)) discussed above, the space scale of damping is obtained from the same positive imaginary parts of the two complex roots, i.e., $b' = \mathrm{Im}k$, with weak magnetic field effects in addition. Figure 8 shows the graphical representation of the normalized penetration depth $\frac{\lambda_{sk}}{c/\omega_p}$ as a function of the normalized deriving frequency ω/ω_p for R- & L-waves, respectively, for $\omega_c/\omega_p = 0.1$ (black), 0.05 (green), and 0.01 (red) and $\mu/T_e = -2, 0, 2$. Observe that the skin depth corresponding to R-wave/L-waves decreases/increases with the increase in the ratio ω_c/ω_p. Again the variation of the curves for different values of ω_c/ω_p is more prominent for $\mu/T_e = -2$ (weak degeneracy). Moreover, the penetration length goes on decreasing for larger values of μ/T_e. Furthermore, the variation of the electromagnetic wave penetration in the presence of ambient magnetic fields is quantitatively large in the regimes where $\mu/T_e < 0$ as compared to other ultra-relativistic regimes.

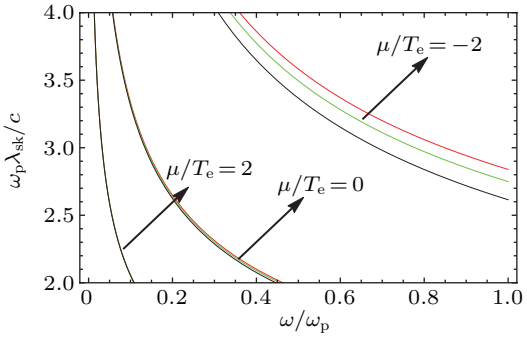

Fig. 8. (color online) Normalized R-mode (solid lines) and L-mode (dashed lines) penetration length $\frac{\lambda_{sk}\omega_p}{c}$ versus normalized frequency $\frac{\omega}{\omega_p}$ for $\omega_c/\omega_p = 0.01$ (red), 0.05 (green), and 0.1 (black).

3. Discussion and summary

We have derived the dispersion relations of parallel propagating electromagnetic waves for ultra-relativistic electron plasma with arbitrary degeneracy. For this purpose, we have

chosen the isotropic ultra-relativistic Fermi–Dirac distribution function. The integral of moments of the Fermi–Dirac distribution function can be expressed in terms of the Polylog function. To compute the integral numerically over the Polylog function, we have used Mathematica (V.9) and obtained the approximated values of the ratios $\mu/E_{\rm F}$, $T/T_{\rm F}$, and $\mu/T_{\rm e}$.

To examine the behavior of the waves, we first obtain the equilibrium number density as a function of the parameter $\mu/T_{\rm e}$ (Fig. 1) and observe that it increases with the increase in $\mu/T_{\rm e}$. We then define the electron plasma frequency $\omega_{\rm p}$ by fixing equilibrium density n_{0e} for $\mu/T_{\rm e}=0$. Figure 2 shows a graphical comparison of the factors $\frac{Li_{2(\mu/T_{\rm e})}}{Li_{3(0)}}$ and $\frac{Li_{1(\mu/T_{\rm e})}}{Li_{3(0)}}$ associated with unmagnetized (Π_{zz} and Π_{xx}) and weakly magnetized (Π_{xy}) components, respectively, of parallel propagating waves for different $\mu/T_{\rm e}$. It is observed that the range $\mu/T_{\rm e}<-1$, in which two curves of the factors $\frac{Li_{2(\mu/T_{\rm e})}}{Li_{3(0)}}$ and $\frac{Li_{1(\mu/T_{\rm e})}}{Li_{3(0)}}$ merge together, in fact leads to the dispersion relations of non-degenerate plasma. The arbitrary degeneracy comes into play when the separation of the curves starts from the range $\mu/T_{\rm e}\geqslant -1$. Moreover, the factor $\frac{Li_{2(\mu/T_{\rm e})}}{Li_{3(0)}}$ associated with the unmagnetized components becomes larger as compared to the factor $\frac{Li_{1(\mu/T_{\rm e})}}{Li_{3(0)}}$ connected with the ambient field. Looking at the dispersion behavior of the principal part of longitudinal and transverse waves plotted in Fig. 3, we observe that, for larger $\mu/T_{\rm e}$, the cutoff frequencies shift upward, the band width between the modes in k-space increases, and the wave propagation becomes weaker. On the other hand, in the range of low phase velocities, the longitudinal Debye screening length (Fig. 4) and transverse penetration depth (Fig. 5) decrease for high arbitrary degeneracy in a field free case. This occurs due to a rise in the electron equilibrium number density.

In the presence of a weak ambient magnetic field, the contribution of the tensor component Π_{xy} is encountered and as a result we obtain the dispersion relation of weakly magnetized R-& L-waves. Figure 6 shows the difference of right and left cutoff points for different arbitrary degenerate environments. This difference, though small in ultra-relativistic regimes, is quantitatively large for negative large values of $\mu/T_{\rm e}$ and goes on decreasing for positive large values. This variation in the strength of the ambient magnetic field can also be observed in the no-propagation case (Fig. 7). The large contribution of the electron cyclotron oscillations can be observed for $\mu/T_{\rm e}=-2$.

In the sublumincal case, the field penetration effect in the presence of weak ambient magnetic field goes on decreasing in case of a right-hand wave and increasing in case of a left-hand wave with the increase of the ratio $\omega_{\rm c}/\omega_{\rm p}$. Moreover, the variation of the curves for different $\omega_{\rm c}/\omega_{\rm p}$ becomes more prominent for $\mu/T_{\rm e}=-2$ (weak degeneracy).

Depending upon the choice of the parameter $\mu/T_{\rm e}$, our results may be useful in various conditions at ultra-high temperatures or densities encountered in modern laser experiments and in various astrophysical situations, for example, stellar, brown dwarf, and giant planet interiors, or the envelopes of neutron stars.

Acknowledgment

H. F. is thankful to Dr. Abdur Rasheed, Assistant Professor GC University Faisalabad Pakistan, for fruitful discussion and encouragement. G. A. acknowledges the grant No. 101/ORIC/17 from the Government College University, Lahore, Pakistan.

References

[1] Bellac M L 1996 *Thermal Field Theory* (Cambridge: Cambridge University Press)
[2] Thoma M H 1995 *Quark-Gluon Plasma 2* (New York: Hwa R C, Ed.) (World Scientific)
[3] Bolton S J 2002 *Nature* **415** 987
[4] Baker D N 2014 *Nature* **515** 531
[5] Shen B and Meyer-ter-Vehn J 2001 *Phys. Rev. E* **65** 016405
[6] Silin V P 1960 *J. Exptl. Theoret. Phys.* **38** 1577
[7] Linhard J 1954 *Kongl. Dan. Vidensk. Selsk. Mat. Fys. Medd.* **28** 8
[8] Laing E W and Diver D A 2013 *Plasma Phys. Control. Fusion* **55** 065006
[9] Shah A, Haque Q and Mahmood S 2011 *Astrophys. Space Sci.* **335** 529
[10] Verdon M W and Melrose D B 2011 *Phys. Rev. E* **83** 056407
[11] Synge J L 1957 *The Relativistic Gas* (Amsterdam: North-Holland)
[12] Chandrasekhar S 1931 *Astrophys. J.* **74** 81
[13] Mamun A A and Shukla P K 2010 *Phys. Plasmas* **17** 104504
[14] Masood W and Eliasson B 2011 *Phys. Plasmas* **18** 034503
[15] Rahman A U, Ali S, Mushtaq A and Qamar A 2013 *J. Plasma Phys.* **79** 817
[16] Shukla P K and Eliasson B 2011 *Rev. Mod. Phys.* **83** 885
[17] Maafa N 1993 *Phys. Scripta* **48** 351
[18] Eliasson B and Shukla P K 2008 *Phys. Scr.* **78** 025503
[19] Melrose D B and Mushtaq A 2010 *Phys. Rev. E* **82** 056402
[20] Melrose D B and Hayes L M 1984 *Aust. J. Phys.* **37** 639
[21] Jancovici B 1962 *Nuovo Cimento* **25** 428
[22] Tsytovich V N 1961 *Sov. Phys. JETP* **13** 1249
[23] Abbas G, Murtaza G and Shah H A 2007 *Phys. Scr.* **76** 649
[24] Abbas G, Murtaza G and Kingham R J 2010 *Phys. Plasmas* **17** 072105
[25] Abbas G, Bashir M F, Ali M and Murtaza G 2012 *Phys. Plasmas* **19** 032103
[26] Abbas G, Bashir M F and Murtaza G 2012 *Phys. Plasmas* **19** 072121
[27] Abbas G, Bashir M F and Murtaza G 2011 *Phys. Plasmas* **18** 102115
[28] Abbas G, Sarfraz M and Shah H A 2014 *Phys. Plasmas* **21** 092108